

1 **Modelling the effect of submarine iceberg melting on glacier-adjacent** 2 **water properties**

3 **Benjamin Davison^{1,2}, Tom Cowton¹, Andrew Sole³, Finlo Cottier^{4,5}, Pete Nienow⁶**

4 ¹Department of Geography and Sustainable Development, University of St Andrews, St Andrews, UK

5 ²School of Earth and Environment, University of Leeds, Leeds, UK

6 ³Department of Geography, University of Sheffield, Sheffield, UK

7 ⁴Scottish Association for Marine Science, Scottish Marine Institute, Oban, UK

8 ⁵Department of Arctic and Marine Biology, UiT The Arctic University of Norway, Tromsø, Norway

9 ⁶School of Geosciences, University of Edinburgh, Edinburgh, UK

10 Correspondence email: b.davison@leeds.ac.uk

11

12 **Abstract**

13 The rate of ocean-driven retreat of Greenland's tidewater glaciers remains highly uncertain in
14 predictions of future sea level rise, in part due to poorly constrained glacier-adjacent water properties.
15 Icebergs and their meltwater contributions are likely important modifiers of fjord water properties, yet
16 their effect is poorly understood. Here, we use a 3-D ocean circulation model, coupled to a submarine
17 iceberg melt module, to investigate the effect of submarine iceberg melting on glacier-adjacent water
18 properties in a range of idealised settings. Submarine iceberg melting can modify glacier-adjacent water
19 properties in three ~~principle~~[principal](#) ways: (1) substantial cooling and modest freshening in the upper
20 ~50 m of the water column; (2) warming of Polar Water at intermediate depths due to iceberg melt-
21 induced upwelling of warm Atlantic Water, and; (3) warming of the deeper Atlantic Water layer when
22 vertical temperature gradients through this layer are steep (due to vertical mixing of warm water at
23 depth), but cooling of the Atlantic Water layer when vertical temperature gradients are shallow. The
24 overall effect of iceberg melt is to make glacier-adjacent water properties more uniform with depth.
25 When icebergs extend to, or below, the depth of a sill at the fjord mouth, they can cause cooling
26 throughout the entire water column. All of these effects are more pronounced in fjords with higher
27 iceberg concentrations and deeper iceberg keel depths. These iceberg melt-induced changes to glacier-
28 adjacent water properties will reduce rates of glacier submarine melting near the surface, but increase
29 them in the Polar Water layer, and cause typically modest impacts in the ~~AW~~[Atlantic Water](#) layer. These
30 results characterise the important role of submarine iceberg melting ~~icebergs~~ in modifying ice sheet-
31 ocean interaction, and highlight the need to improve representations of fjord processes in ice sheet-scale
32 models.

33

34 **1. Introduction**

35 Predicting the rates of ocean-driven retreat of Greenland's tidewater glaciers remains one of the largest
36 uncertainties in estimating future sea level rise (Edwards et al., 2021; Meredith et al., 2020). This
37 uncertainty is partly due to limited constraints on the ocean-driven thermal forcing of tidewater glacier
38 calving fronts, which reflects in part the difficulty in obtaining hydrographic observations in the
39 proximity of tidewater glacier termini (Jackson et al., 2017, 2020; Sutherland et al., 2019). The few
40 observations of water properties in the inner part of glacial fjords demonstrate that there are typically
41 substantial differences between glacier-adjacent water properties and those near the fjord mouth (e.g.
42 Inall et al., 2014; Jakobsson et al., 2020; Straneo et al., 2011), indicating that substantial modification
43 of water temperature and salinity can occur within glacial fjords. Due to the relatively small number of
44 observations and insufficient model constraints on glacier-adjacent water properties, ice sheet models
45 used to simulate glacier retreat must be forced with far-field (i.e. acquired on and beyond the continental
46 shelf) ocean boundary conditions that do not include fjord-scale influences (Goelzer et al., 2020; Slater
47 et al., 2019), thereby introducing uncertainty into the resulting projections of ice sheet mass loss.

48 Glacier-adjacent water properties can differ from those near the fjord mouth for several reasons.
49 Meltwater runoff enters the fjord at depth where tidewater glaciers meet the ocean ('subglacial
50 discharge'). In Greenland's fjords, warm water of Atlantic origin (Atlantic Water, AW) is generally
51 found at depth, whilst colder, fresher water of Polar origin (Polar Water, PW) is found at intermediate
52 depths (Straneo and Heimbach, 2013; Sutherland and Pickart, 2008). The cold, fresh subglacial
53 discharge is buoyant when it enters the fjord, so rises as a turbulent plume (Jenkins, 2011). As it rises,
54 it entrains fjord water, which mixes with the subglacial discharge as it ascends towards the fjord surface
55 (e.g. Beaird et al., 2018). In this way, subglacial discharge-driven plumes act as mixing engines at the
56 head of glacial fjords. Due to the temperature stratification in Greenland's fjords, plumes at deeply-
57 grounded glaciers (i.e. deeper than the PW-AW interface) often draw the relatively warm AW towards
58 the fjord surface, thereby warming surface and near-surface waters (e.g. Carroll et al., 2016; Straneo et
59 al., 2010, 2011). In contrast, plumes at shallowly-grounded glaciers can cause cooling at and near the
60 fjord surface, as cold subglacial discharge and entrained PW is upwelled into surface layers that are
61 seasonally warmed by solar radiation (Carroll et al., 2016). Models that include glacial plumes are able
62 to reproduce these effects convincingly (Carroll et al., 2016; Cowton et al., 2015; Jackson et al., 2017).
63 However, there remain substantial differences between modelled water properties and those that are
64 observed adjacent to tidewater glaciers (Cowton et al., 2016; Davison et al., 2020; Fraser and Inall,
65 2018).

66 Several recent studies have identified icebergs as a substantial freshwater source in some of Greenland's
67 fjords, with iceberg freshwater volumes comparable to or greater than ice sheet runoff (Enderlin et al.,
68 2016, 2018; Jackson and Straneo, 2016; Moon et al., 2017; Moyer et al., 2019; Rezvanbehbahani et al.,
69 2020). Furthermore, modelling of one of these fjords suggests that including the heat and salt fluxes

70 associated with submarine iceberg melting increases greatly the model's ability to reproduce observed
71 glacier-adjacent water properties (Davison et al., 2020). However, iceberg concentration, keel depth,
72 and size-frequency distribution likely vary hugely between fjords as well as over time, though
73 observations of icebergs at the fjord scale are sparse (Enderlin et al., 2016; Moyer et al., 2019;
74 Rezvanbehbahani et al., 2020; Sulak et al., 2017). As such, it is likely that the effect of icebergs on
75 glacier-adjacent water properties will also vary both spatially (i.e. between fjords) and temporally. This
76 variability likely results in different thermal forcing of tidewater glaciers for a given set of far-field
77 ocean conditions. Constraining the effect of icebergs on glacier-adjacent water properties, and thus
78 glacier submarine melt rates, is therefore a necessary step in order to improve projections of ice sheet
79 mass loss.

80 Here, we use an ocean circulation model in a series of idealised fjord-scale simulations to examine how
81 icebergs affect glacier-adjacent water properties across a range of Greenland-relevant scenarios. We
82 first consider how iceberg concentration, keel depth and size-frequency distribution individually affect
83 glacier-adjacent water properties. We then consider a range of representative iceberg and ocean
84 scenarios, to examine how these parameters interact to determine water properties in the critical region
85 adjacent to tidewater glacier termini. Greenland's fjords are complex and varied in their geometry,
86 ranging from short, narrow inlets to those that are long and wide, each with varying sinuosity and
87 bathymetry, and often with several tributaries and sills of varying depth along their length. It would be
88 impractical to attempt to characterise all of these systems. Therefore, we focus here on two simple fjord
89 geometries: one with no sills and another with a single entrance sill, which we expect to be of particular
90 importance for iceberg-ocean interaction given the capacity of sills to concentrate fjord-shelf water
91 exchange near the surface where icebergs are concentrated- ([Schaffer et al., 2020](#)).

92

93 **2. Methods**

94 **2.1. Model domain**

95 We use the Massachusetts Institute of Technology general circulation model (MITgcm) in its non-
96 hydrostatic configuration (Marshall et al., 1997a, 1997b) to model submarine ice melting and circulation
97 in an idealised fjord 50 km in length and 5 km in width. In most simulations, the domain is uniformly
98 500 m deep. However, in some simulations, we include a sill which limits the overlying water depth to
99 100 m (uniform across the entire width of the fjord, and approximately 5 km wide in the along-fjord
100 direction, with a Gaussian profile), centred 10 km from the open boundary (Fig. 1a). Model resolution
101 is uniformly 500 m horizontally and 10 m vertically. The fjord sides are closed boundaries, while at the
102 open ocean boundary we impose a 5 km sponge layer, in which conditions are relaxed towards those
103 imposed at the boundary (e.g. Cowton et al., 2016; Sciascia et al., 2013; Slater et al., 2015). The glacier-
104 end of the domain is closed and consists of a virtual ice wall 5 km wide and 500 m high. In simulations

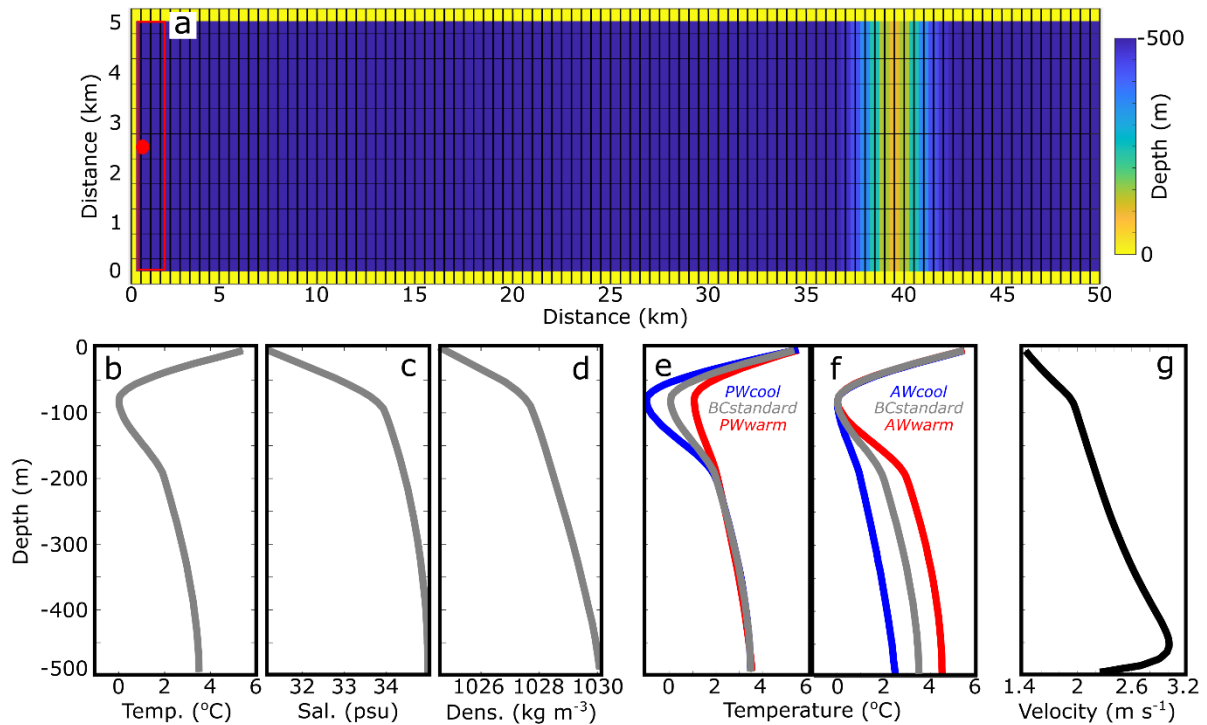


Figure 1. Model domain and boundary conditions. (a) Plan-view of model bathymetry with sill, with the ice wall at the left end of the domain (0 km) and the open boundary on the right. Hatching indicates model resolution (note that grid cells are 500 m x 500 m in the horizontal). The red dot marks the location of subglacial discharge injection and the red box indicates the region from which steady-state glacier-adjacent water properties were extracted. In simulations without a sill, the domain is uniformly 500 m deep. Vertical profiles of (b) temperature, (c) salinity and (d) density with *BCstandard*. (e) Temperature profiles with varying PW temperature. (f) Temperature profiles with varying AW temperature. (g) Example plume vertical velocity from the simulation with iceberg scenario five, 500 m³ s⁻¹ subglacial discharge and *BCstandard* boundary conditions.

105 incorporating [runoffsubglacial discharge](#), this is input at a rate of 500 m³ s⁻¹, a value typical of many of
 106 Greenland's tidewater glaciers (Mankoff et al., 2020), at the centre of the base of the ice wall (Fig. 1a).
 107 The velocity of the [runoffsubglacial discharge](#)-driven plume (e.g. Fig. 1g) and the melting of the ice
 108 wall were calculated using the 'IcePlume' package (Cowton et al., 2015). In common with several
 109 previous studies (Kimura et al., 2014; Slater et al., 2015; Xu et al., 2013), we implement a free slip
 110 condition on the fjord walls and ice front [and do not simulate the effects of sea ice, atmospheric forcing](#)
 111 [or tides](#).

112 2.2. Initial and open boundary conditions

113 We use idealised representations of temperature and salinity profiles commonly observed at the mouth
 114 of Greenland's south-eastern fjords during late-summer as initial and open boundary conditions
 115 (Sutherland et al., 2014). In our standard setup, this idealised profile is a cubic interpolation between
 116 6°C and 31 psu at the fjord surface, 0°C and 34 psu at 100 m depth, 2°C at 200 m and 3.5°C at 500 m
 117 depth, where salinity is greatest at 35 psu (Fig. 1b-d). In this way, the upper several tens of metres

118 represent waters that are seasonally warmed by solar insolation, whilst the relatively cold intermediate
119 layer, centred 100 m below the fjord surface, represents the PW layer, which is underlain by warmer,
120 more saline water representing the AW layer. Henceforth, we refer to this set of boundary conditions
121 as *BCstandard*. In separate simulations, we use temperature minima at 100 m of -1°C (*PWcool*) and
122 1°C (*PWwarm*) and temperature maxima at 500 m of 2.5°C (*AWcool*) and 4.5°C (*AWwarm*) (Fig. 1e,f).
123 Changing the temperature of the AW and PW layers causes corresponding changes in the vertical
124 temperature gradient (Fig. 1e,f), the effects of which are discussed in Sect. 3.2. Initial and open
125 boundary salinity are kept constant between simulations, but density changes between simulations are
126 negligible. Boundary conditions were kept constant throughout each simulation. We focus on late-
127 summer ocean conditions because of the greater availability of observations at that time to both force
128 the model and with which to make comparisons.

129

130 **2.3. Iceberg-ocean interaction**

131 Submarine iceberg melting is simulated using the ‘IceBerg’ package within MITgcm (Davison et al.,
132 2020), with an ice temperature of -10°C (Inall et al., 2014; Luthi et al., 2002; Sciascia et al., 2013;
133 Sutherland and Straneo, 2012). ~~This package uses the velocity-dependent three-equation melt rate~~
134 ~~parameterisation (Holland and Jenkins, 1999; Xu et al., 2012), with standard parameter values (Cowton~~
135 ~~127 et al., 2015; Davison et al., 2020; Jackson et al., 2020) for the drag coefficient (0.0025), and thermal~~
136 ~~128 and salt turbulent transfer coefficients (0.022 and 0.00062, respectively). The icebergs are~~
137 ~~rectangular 129 in plan view and have flat, vertical sides. All icebergs have length, l , to width ratios of~~
138 ~~1.62:1 130 (Dowdeswell et al., 1992), and iceberg keel depth, d , is related to iceberg length through,~~
139 ~~$d=2.911071$ 131 (Barker et al., 2004).~~This package uses the velocity-dependent three-equation melt rate
140 parameterisation (Hellmer and Olbers, 1989; Holland and Jenkins, 1999; Xu et al., 2012). We chose to
141 use this melt rate parameterisation, rather than existing iceberg melt parameterisations (e.g. Bigg et al.,
142 1997), because it enables us to resolve the vertical pattern of submarine melting of individual icebergs.
143 The temperature and salinity fluxes associated with melting of individual iceberg faces within a grid
144 cell are calculated based on local temperature, salinity and face-normal velocity. Face-normal current
145 speed is calculated assuming that icebergs drift with the average current velocity along their draught
146 (though we note that the iceberg locations are kept constant through each simulation). Melt-driven
147 plumes are not simulated directly; instead, their effect on melt rates is parameterised by applying a
148 minimum face-normal current speed of 0.06 m s^{-1} to each iceberg face. This minimum current speed is
149 based on line plume modelling (Davison et al., 2020). The package does not include the effect of waves
150 or mechanical iceberg breakup; therefore, melt rates calculated here are conservative. We use standard
151 parameter values (Cowton et al., 2015; Davison et al., 2020; Jackson et al., 2020) for the drag coefficient
152 (0.0025), and thermal and salt turbulent transfer coefficients (0.022 and 0.00062, respectively). The
153 icebergs are rectangular in plan-view and have flat, vertical sides. All icebergs have length, l , to width

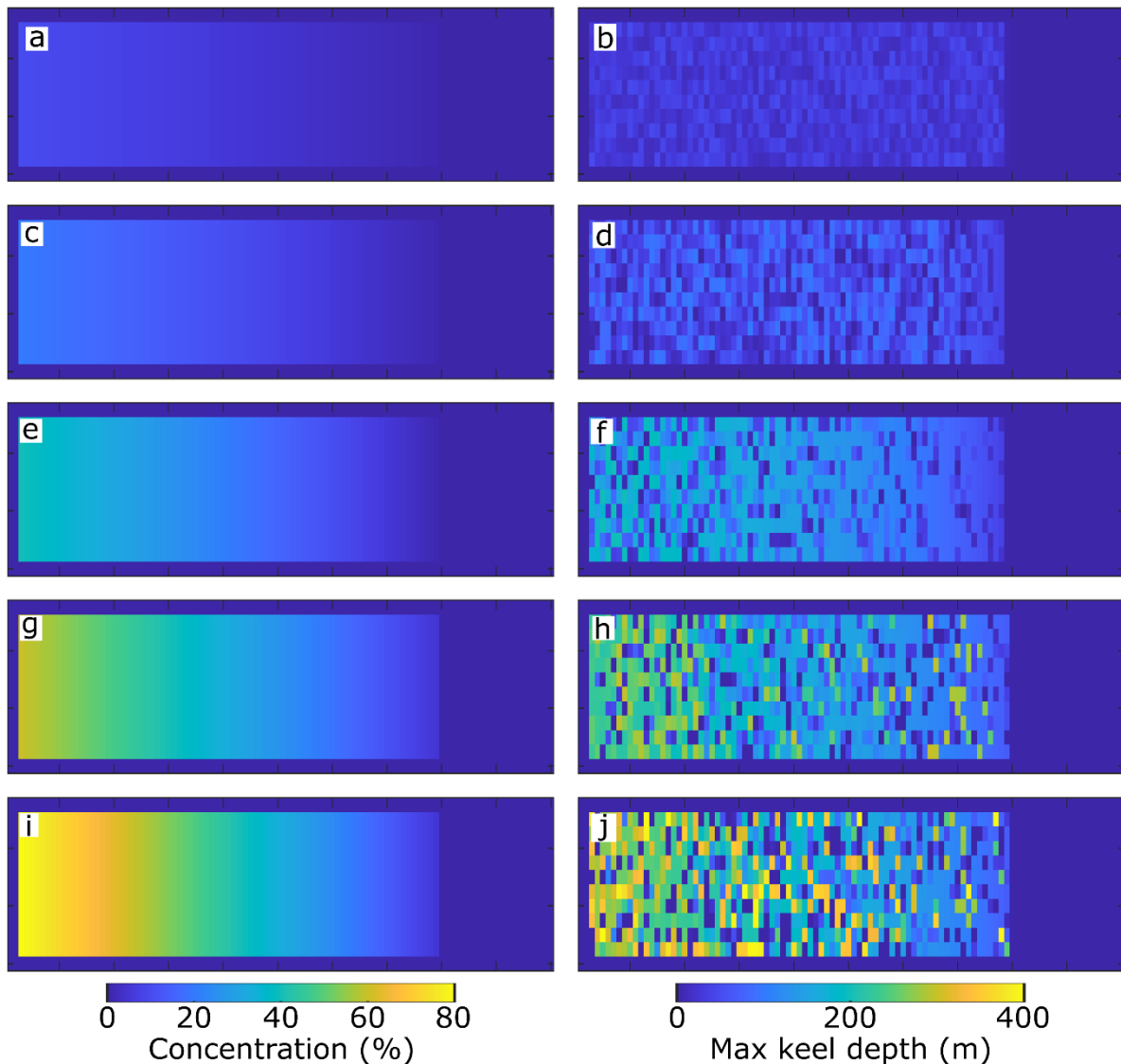


Figure 2. Iceberg concentration (left column) and maximum iceberg keel depth (right column) for iceberg scenarios one to five (top to bottom). All panels show the domain in plan-view, and are 50 km long and 5 km across.

154 [ratios of 1.62:1 \(Dowdeswell et al., 1992\), and iceberg keel depth, \$d\$, is related to iceberg length through,](#)
 155 [\$d=2.91l^{0.71}\$ \(Barker et al., 2004\).](#)

156 In Sect. 3.1, we consider a range of iceberg concentrations, maximum keel depths and size-frequency
 157 distributions, whilst using only the *BCstandard* boundary conditions. In all setups, iceberg
 158 concentration is uniform across the fjord and decreases linearly from a maximum adjacent to the virtual
 159 ice wall to a minimum 10 km from the open boundary. In Sect. 3.1, iceberg concentration (defined as
 160 the percentage of the fjord surface in plan-view occupied by icebergs), is 80% adjacent to the ice wall
 161 and decreases to 5% in our *c1₇* experiment, and is reduced to 75, 50 and 25% of these values in our
 162 *c0.75*, *c0.5*, and *c0.25* experiments, respectively. Regardless of concentration, we use a maximum

Table 1. Details of each iceberg scenario. Concentration is the percentage of the fjord in plan-view occupied by icebergs. Iceberg concentration was linearly interpolated from the maximum value (adjacent to the glacier wall) to the minimum value 40 km down fjord.

Iceberg scenario	Max. draught (m)	Exponent	Concentration [max,min] (%)	Surface area (km ²)
Scenario 1	50	1.6	[10,1]	44.5
Scenario 2	100	1.7	[20,1]	76.5
Scenario 3	200	1.8	[40,1]	141
Scenario 4	300	1.9	[60,5]	235
Scenario 5	400	2.1	[80,5]	316

163 iceberg keel depth of 300 m and the size-frequency distribution of the icebergs is described using a
 164 power law with an exponent of -2, which is similar to that observed in Sermilik Fjord (Sulak et al.,
 165 2017). In separate simulations, we assign maximum iceberg keel depths of 50 m, 150 m, 250 m, 350 m
 166 and 450 m, whilst maintaining the cI concentration and the -2 power law exponent. We then vary the
 167 size-frequency distribution power law exponent from -1.6 to -2.1 in increments of 0.1 (covering the
 168 range observed to date in Greenland’s fjords (Rezvanbehbahani et al., 2020; Sulak et al., 2017)), whilst
 169 retaining the cI concentration and the 300 m maximum keel depth. [In this section \(Sect. 3.1\) we show](#)
 170 [results from simulations both with and without subglacial discharge, to demonstrate the effect of](#)
 171 [icebergs in isolation and in combination with subglacial discharge.](#)

172 In Sect. 3.2 onwards, we consider five realistic combinations of iceberg concentration, maximum
 173 iceberg keel depth and power law exponent, in order to approximate the range of iceberg geometries
 174 and distributions found in Greenland’s fjords ([Fig. in summer \(Fig. 2\). In these setups, iceberg](#)
 175 [concentration decreases linearly in the along-fjord direction away from the glacier between specified](#)
 176 [maximum and minimum values \(Table 1\) and icebergs are distributed randomly in the across-fjord](#)
 177 [direction \(Fig. 2\).](#) These iceberg setups range from those representing a fjord hosting few and small
 178 icebergs, such as Kangerlussuup Sermia Fjord (Sulak et al., 2017) (scenario one), to those representing
 179 an iceberg-congested fjord, such as Sermilik Fjord (scenario five) (Fig. 2; Table 1). [In all simulations](#)
 180 [shown in this section \(Sect. 3.2\) 500 m³ s⁻¹ subglacial discharge is injected into the fjord as described](#)
 181 [in Section 2.1.](#)

182

183 3. Results

184 3.1. The effect of iceberg concentration, keel depth and size-frequency distribution on glacier- 185 adjacent water properties

186 The effect of iceberg melt on glacier-adjacent water properties depends on iceberg geometry, iceberg
 187 concentration and iceberg size-frequency distribution (Fig. 3), as well as on the presence or absence of
 188 subglacial discharge. In the absence of subglacial discharge, icebergs modify glacier-adjacent water

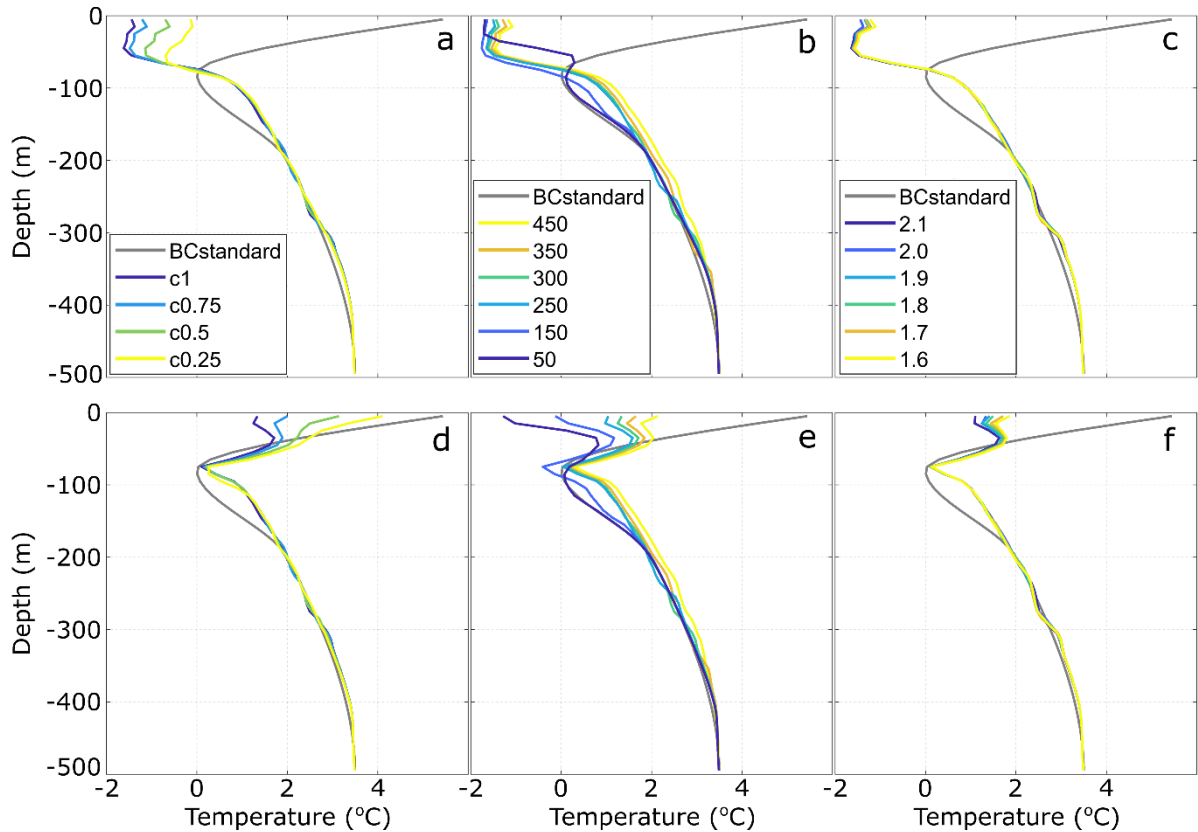


Figure 3. Glacier-adjacent water temperature vs iceberg geometry and distribution. Effect of iceberg concentration (a & d), maximum iceberg draught (b & e) and exponent describing the size-frequency distribution (c & f). Panels (a-c) are for simulations without subglacial discharge, whilst panels (d-f) are for simulations with $500 \text{ m}^3 \text{ s}^{-1}$ subglacial discharge.

189 properties (here defined as the average properties of the water within 2 km of the ice wall; Fig. 1a) in
 190 two main ways. Firstly, they cause substantial ($6\text{-}7.5^\circ\text{C}$) cooling in the upper ~ 60 m of the water column,
 191 relative to the initial conditions (Fig. 3a-c). The amount of cooling in this near-surface layer depends
 192 somewhat on iceberg concentration, with steady-state water temperature varying between $\sim -1.5^\circ\text{C}$ and
 193 $\sim 0^\circ\text{C}$ over the range of iceberg concentrations considered, but is otherwise relatively insensitive to
 194 changing iceberg geometry and distribution (Fig. 3a-c). Secondly, warming of up to $\sim 1^\circ\text{C}$ occurs below
 195 ~ 80 m because iceberg melting causes localised freshening at depth. The resulting iceberg melt-
 196 modified water (i.e. the mixture of iceberg freshwater and ambient water at depth) is less dense than the
 197 surrounding water and rises buoyantly towards the fjord surface. The vertical extent and magnitude of
 198 the resulting warming generally increase with maximum iceberg keel depth (Fig. 3b), because icebergs
 199 with deeper keels cause upwelling of deeper AW (which in this case is also warmer (Fig. 1b)). This
 200 warming effect does not extend to the fjord surface, because the stronger stratification near the surface
 201 limits upwelling and because iceberg-ocean contact areas are much greater near the surface, so cooling
 202 due to localised iceberg melting dominates. When subglacial discharge is included, the effect of iceberg

203 melt on glacier-adjacent water properties at depth (below 60 m) is similar to that in simulations without
204 subglacial discharge, but glacier-adjacent water temperatures in the upper ~60 m of the water column
205 display a greater range and the cooling of the near-surface waters is considerably reduced (Fig. 3d-f).
206 This is because the [runoff/subglacial discharge](#) causes strong upwelling of AW towards the fjord surface
207 and increases rates of fjord-shelf exchange, which counters some of the iceberg-induced cooling of
208 near-surface waters.

209

210 **3.2. Combining iceberg scenarios and ocean conditions**

211 In reality, changes in iceberg concentration, keel depth and size-frequency distribution do not occur in
212 isolation and there are characteristic relationships between those iceberg descriptors (Sulak et al., 2017).
213 Fjords hosting large glaciers, such as Sermilik Fjord and Helheim Glacier in east Greenland, tend to
214 contain both high iceberg concentrations and large, deeply-draughted icebergs, whilst those with lower
215 iceberg concentrations, such as Kangerlussuup Sermia Fjord, also tend to contain smaller icebergs. To
216 better represent the range of iceberg conditions found in Greenland's fjords, we consider five iceberg
217 'scenarios' (Fig. 2; Table 1), ranging from a fjord with low iceberg concentration, shallow iceberg keels
218 and fairly uniform iceberg sizes (iceberg scenario one), to a fjord with high iceberg concentration, deep
219 iceberg keels and a large range of iceberg sizes (iceberg scenario five). For each of these scenarios, we
220 examine steady-state glacier-adjacent water temperature for a range of ocean boundary conditions, and
221 with and without a shallow (100 m) sill. We therefore consider three different PW and AW temperatures
222 in turn (Fig. 1e,f), and examine the resulting glacier-adjacent water properties for each of the five
223 iceberg scenarios. To isolate the effect of iceberg melting from other processes, we compare each of the
224 above simulations to identical simulations without icebergs.

225

226 **3.2.1. Changing Polar Water temperature**

227 Fig. 4 shows steady-state glacier-adjacent water properties for the range of iceberg scenarios and PW
228 temperatures considered. In all iceberg scenarios, there is substantial (~2°C or more) cooling in the
229 upper ~60 m, with greater cooling in scenarios with higher iceberg concentrations. Other than this near-
230 surface cooling, glacier-adjacent water properties are very similar to open ocean conditions in iceberg
231 scenarios one and two (which have the lowest iceberg concentrations; Fig. 2; Table 1). However, in
232 iceberg scenarios three to five, the PW layer is increasingly modified (Fig.s 4c-e). With *PWcool*,
233 icebergs in these scenarios cause on average a net *warming* of 1.02°C in the 80-200 m depth range,
234 compared to simulations without icebergs. Conversely, with *PWwarm*, the icebergs cause a net cooling
235 of 0.30°C over the same depth range, such that the steady-state temperature profiles for both sets of
236 initial conditions (*PWcool* and *PWwarm*) are similar. With *BCstandard*, the influence of icebergs on
237 glacier-adjacent water properties falls between the two, with the net effect being a slight (0.43°C)

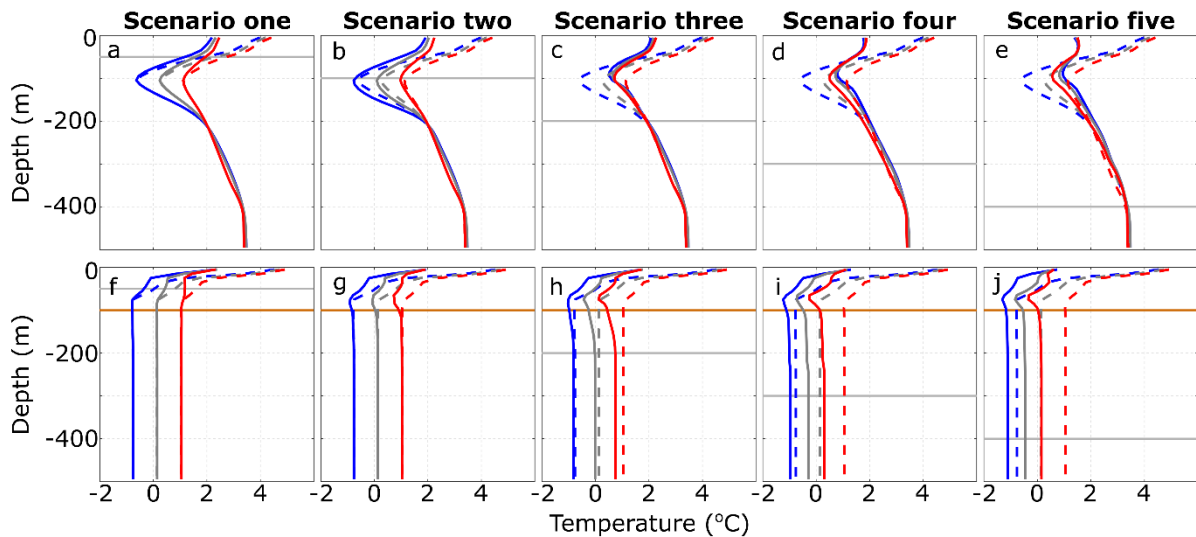


Figure 4. Steady-state glacier-adjacent water temperature for a range of initial Polar Water conditions. In all plots, solid and dashed lines indicate simulations with and without icebergs, respectively. Plots a-e show configurations with a flat-bottomed domain, whilst f-j show those with a 100 m deep sill. Grey, blue and red lines show scenarios using the *BCstandard*, *PWcool* and *PWwarm* boundary conditions respectively (shown in Figure 1e). The horizontal grey lines indicate the maximum iceberg keel depth in each scenario, and the horizontal orange lines in panels f-j indicate the sill depth.

238 warming (Fig. 4c-e). These changes arise due to differing balances between cooling due to iceberg
 239 melting, and warming due to buoyancy-induced upwelling of relatively warm AW water. With *PWcool*
 240 there is relatively little iceberg melting in the PW layer (because the PW is close to the *in-situ* freezing
 241 point), and so warming due to upwelling of AW dominates (driven by iceberg melting at greater depth
 242 in the warmer AW layer). In contrast, with *PWwarm*, iceberg melt rates in the PW layer are
 243 comparatively high, and the temperature difference between the PW and AW layers is reduced, so
 244 localised cooling offsets warming due to turbulent upwelling. In short, under the conditions represented
 245 by these simulations, submarine iceberg melting acts to make glacier-adjacent water temperature more
 246 uniform with depth (Fig. 4c-e).

247 The addition of a 100 m deep sill near the fjord mouth serves to amplify the cooling effect of icebergs
 248 (Fig. 4f-j). Sills typically block external shelf waters below the sill depth from entering the fjord (unless
 249 external forcing causes a shallowing of isopycnals seaward of the sill), causing the fjord basin bounded
 250 by the sill to be replenished by waters sourced only from above the sill depth (e.g. Jakobsson et al.,
 251 2020). When icebergs reach down to the sill depth, all water entering the fjord may thus be subject to
 252 melt-driven cooling. The result is that icebergs cause cooling throughout the water column, even below
 253 the deepest iceberg keels and below the sill depth (Fig. 4f-j). This cooling is increasingly pronounced
 254 as the PW temperature increases and with more concentrated and deeper icebergs (Fig. 4f-j). For
 255 example, over the 100 to 500 m depth range with *PWcool*, icebergs cause 0.21°C cooling on average in

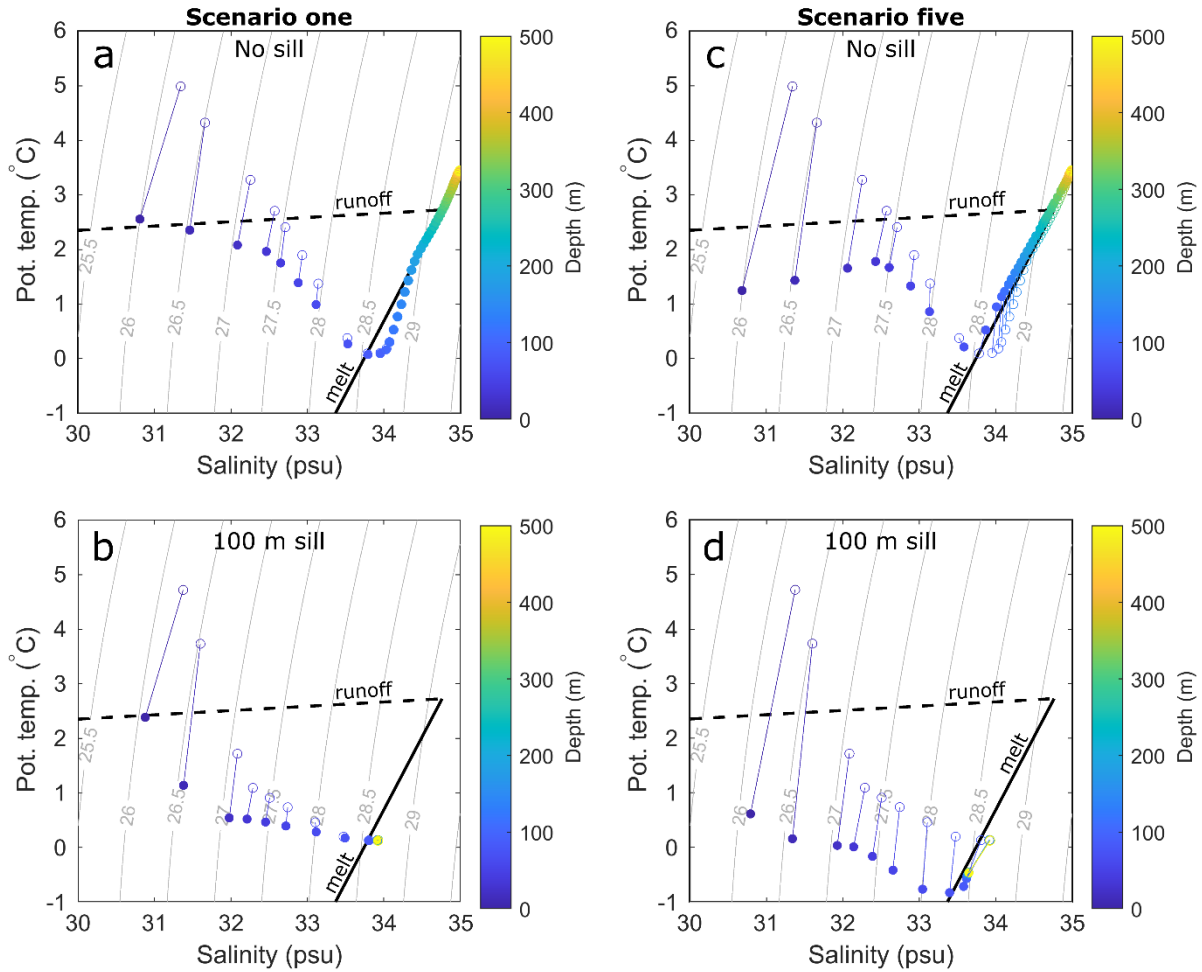


Figure 5. Glacier-adjacent temperature and salinity with (solid circles) and without icebergs (open circles) for various iceberg and sill scenarios and with *BCstandard* boundary conditions. Panels (a) and (b) show iceberg scenario one without a 100 m sill (a) and with a sill (b). Panels (c) and (d) show iceberg scenario five, without a sill (c) and with a 100 m sill (d). Solid lines joining open and closed circles indicate connected data points extracted from the same model depth.

256 iceberg scenarios three to five (0.06°C in scenario three and 0.35°C in scenario five); whilst with
 257 *PWwarm*, icebergs cause 0.67°C cooling on average (0.33°C in scenario three and 0.91°C in scenario
 258 five).

259 The varied effects of icebergs on glacier-adjacent water properties are apparent in temperature-salinity
 260 space (Fig. 5). Initial glacier-adjacent water properties are inherited from those prescribed at the fjord
 261 mouth; however, icebergs modify fjord waters through ice melt and meltwater-driven vertical mixing.
 262 Comparing temperature-salinity profiles of simulations with and without icebergs illustrates these
 263 effects (Fig. 5). In the upper ~ 60 m of all simulations with icebergs, iceberg melting causes substantial
 264 cooling and slight freshening (e.g. compare solid and open circles in Fig. 5 – solid circles are drawn
 265 down and slightly left in temperature-salinity space). Deeper in the water column (below 100 m), the
 266 influence of iceberg melting on water properties depends on the iceberg scenario and the presence or
 267 absence of a sill. In iceberg scenario one (Fig. 5a, b), iceberg melting causes very little modification of

268 waters below 100 m, even in the presence of a sill (Fig. 5b). This is because the icebergs do not extend
269 to the sill water depth and so there is some unmodified exchange between the fjord and shelf. In iceberg
270 scenario five, icebergs cause on average 0.19°C warming of waters below 100 m when there is no sill,
271 and cooling of 0.61°C below 100 m when there is a sill (Fig. 5b). This cooling below the maximum
272 iceberg draught occurs in all iceberg scenarios in which icebergs extend to sill depth, but is most
273 apparent in the higher iceberg concentration scenarios (e.g. Fig. 5d). The simulated changes in water
274 properties arise due the combined effects of local iceberg melting and fjord circulation. Submarine
275 iceberg melting reduces the density of surrounding waters, causing upwelling until those waters
276 equilibrate at a new neutral buoyancy depth with respect to the fjord stratification. Within the
277 temperature-salinity space of Greenland's fjords, density is predominantly salinity controlled.
278 Therefore, the salinity stratification is little changed by iceberg melting, whilst the temperature changes
279 are much more pronounced. This means that the iceberg melt-induced migrations through temperature-
280 salinity space that are often steeper than predicted by the submarine melt mixing line (Gade, 1979).

281

282 **3.2.2. Changing Atlantic Water temperature**

283 We also examine the interactions between iceberg scenarios and changes to AW temperature (Fig. 6).
284 As in the PW scenarios, there is always marked cooling in the upper ~60 m of the water column and
285 water modification below this is minimal for iceberg scenarios one and two. In iceberg scenarios three
286 to five, icebergs penetrate to a greater depth and thus into the AW layer, releasing freshwater which
287 causes upwelling of AW. In these cases, the net effect of icebergs on water properties between ~80 m
288 and the maximum iceberg keel depth depends on the balance between cooling due to localised iceberg
289 melting, and warming due to upwelling of AW. With *AWwarm*, there is a steep temperature gradient
290 between the cold PW and warmer AW layers. Consequently, upwelling of AW causes notable warming
291 in the PW layer that offsets localised iceberg-induced cooling. In the scenarios with greater iceberg
292 concentration (e.g. iceberg scenario five; Fig. 6e), the icebergs penetrate deeper into the AW layer and
293 so can induce upwelling of the deeper, warmer water, resulting in more warming and over a greater
294 depth range than in the lower iceberg concentration scenarios. However, with *AWcool*, the vertical
295 temperature gradient is reduced, so cooling due to localised iceberg melting dominates the signal
296 between the maximum iceberg draught and ~80 m.

297 This dependence of iceberg modification of glacier-adjacent water properties on the temperature
298 gradient through the AW layer is further illustrated by sensitivity tests in which the temperature of the
299 AW layer was modified in two ways relative to *BCstandard*. First, to examine whether the absolute
300 temperature of the water column affected the balance between upwelling and melting, the entire water
301 column was uniformly warmed by 1°C. With this uniform shift in temperature, the pattern of
302 temperature with depth is similar to that of *BCstandard* (compare dashed grey and red lines in Fig. 7b),

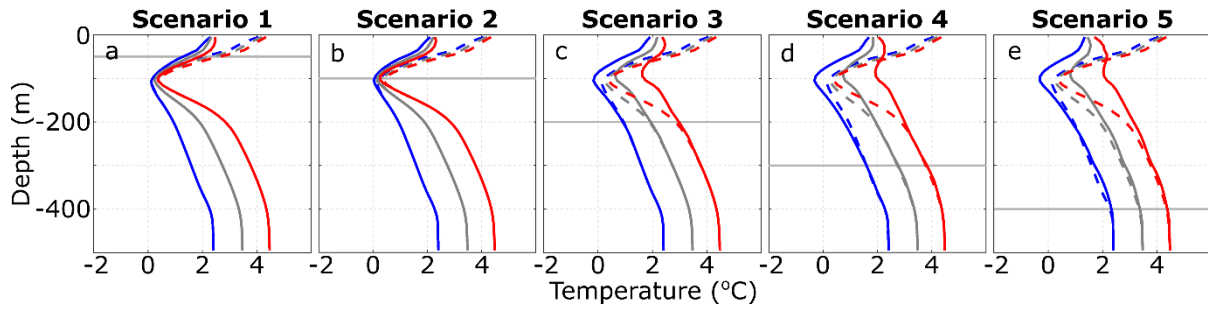


Figure 6. Steady-state glacier-adjacent water temperature for a range of initial Atlantic Water conditions and with a flat-bottomed domain. In all plots, solid and dashed lines indicate simulations with and without icebergs, respectively. Grey, blue and red lines show scenarios using the *BCstandard*, *AWcool* and *AWwarm* boundary conditions, respectively (shown in Figure 1f). The horizontal grey lines indicate the maximum iceberg keel depth in each scenario.

303 illustrating that the additional upwelling-driven warming with *AWwarm* is due to the steeper
 304 temperature gradient between the PW and AW layers, rather than the absolute temperature of the AW.
 305 Secondly, to illustrate the importance of the temperature gradient within the AW layer, we made the
 306 AW layer uniformly 3.5°C. With this set of boundary conditions, upwelling-driven warming dominates
 307 in the PW layer, because of upwelling of warm AW, whilst melt-driven cooling dominates in the AW
 308 layer because upwelling-driven warming is muted (Fig. 7c). Thus, the average warming below ~80 m
 309 that we simulate with *AWwarm* is strongly sensitive to the vertical temperature gradient, and not only
 310 the average or maximum temperature of the AW.

311 With the addition of a 100 m sill, AW does not propagate into the fjord under the conditions simulated
 312 here. Thus in steady-state, glacier-adjacent water properties are unaffected by AW and adopt the
 313 properties of the PW layer (modified by iceberg melting and ~~runoff~~-subglacial discharge). The resulting
 314 profiles therefore resemble the dashed pale blue lines in Fig. 4f-j and are not shown here.

315

316 4. Discussion

317 4.1. Comparison with observations and applicability to real fjords

318 Our simulations suggest that several changes to glacier-adjacent water properties can occur due to
 319 submarine iceberg melting. In almost all simulations, we simulate pronounced ($>2^{\circ}\text{C}$) cooling in the
 320 upper several tens of metres of the water column. Deeper in the water column (between ~80 m and the
 321 maximum iceberg keel depth), both iceberg-induced cooling and warming can occur (e.g. Fig. 4 and 6),
 322 depending on the balance between cooling due local iceberg melting and warming due to melt-driven
 323 upwelling. The balance between these processes depends on the iceberg contact area at depth available
 324 for local melting (and therefore cooling) and on the temperature of the upwelling water. When vertical
 325 temperature gradients are steep (e.g. with *AWwarm*; Fig. 6), icebergs can cause warming between their

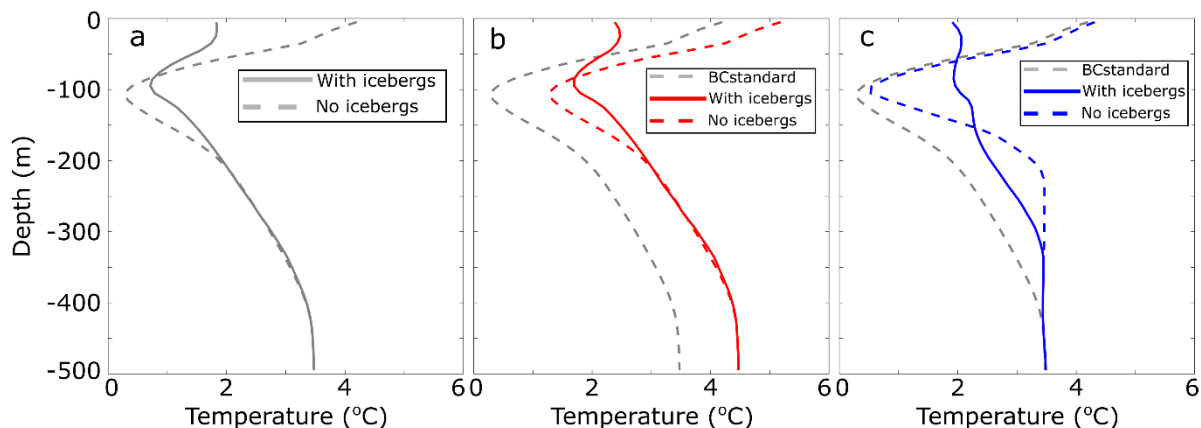


Figure 7. AW temperature gradient sensitivity tests. Panels show simulations using (a) *BCstandard*, (b) temperature profile shifted by 1°C throughout the water column, and (c) uniform initial AW temperature of 3.5°C. Steady-state conditions without icebergs using *BCstandard* (grey line) are also shown in (b) and (c) for reference.

326 maximum keel depth and the surface layer. This is particularly apparent in the PW layer, where the
 327 temperature difference between an upwelled parcel of water and that at the parcel’s new neutral
 328 buoyancy depth in the PW layer is greatest, and where iceberg melt rates (and therefore melt-driven
 329 cooling) are generally smaller because of the low water temperatures. In contrast, when vertical
 330 temperature gradients are shallower (e.g. with *AWcool*), cooling due to localised melting dominates
 331 (blue lines in Fig. 7d,e and 7c). These effects tend to reduce vertical temperature variations of glacier-
 332 adjacent waters compared both to simulations without icebergs and compared to conditions at the fjord
 333 mouth.

334 Detailed near-glacier hydrographic observations against which to make comparisons are sparse, but
 335 those that do exist provide some useful insight into the applicability of our model results to Greenland’s
 336 fjords. The pronounced surface and near-surface cooling (relative to conditions at the mouth) that we
 337 simulate is a common feature in Greenland’s fjords. For example, a transect of conductivity,
 338 temperature, depth (CTD) casts along Sermilik Fjord revealed cooling of approximately 4°C in the
 339 upper ~50 m (Straneo et al., 2011, 2012), which was also reproduced in a detailed modelling study of
 340 Sermilik Fjord that included icebergs (Davison et al., 2020). Similar along-fjord near-surface cooling
 341 has also been observed in other iceberg-congested fjords, such as Illulissat Isfjord (Beaird et al., 2017;
 342 Gladish et al., 2015) and Upernavik Isfjord (Fenty et al., 2016), both in west Greenland. In Illulissat
 343 Isfjord, the cold surface layer usually extends along-fjord to a shallow sill at the fjord mouth, where
 344 icebergs frequently become grounded (Gladish et al., 2015).

345 Iceberg-induced changes to water properties below ~80 m are harder to identify in hydrographic
 346 observations, most likely because they also contain the signature of glacial-plumes resulting from
 347 subglacial discharge, or other external forcings. Our modelling suggests that, if vertical temperature

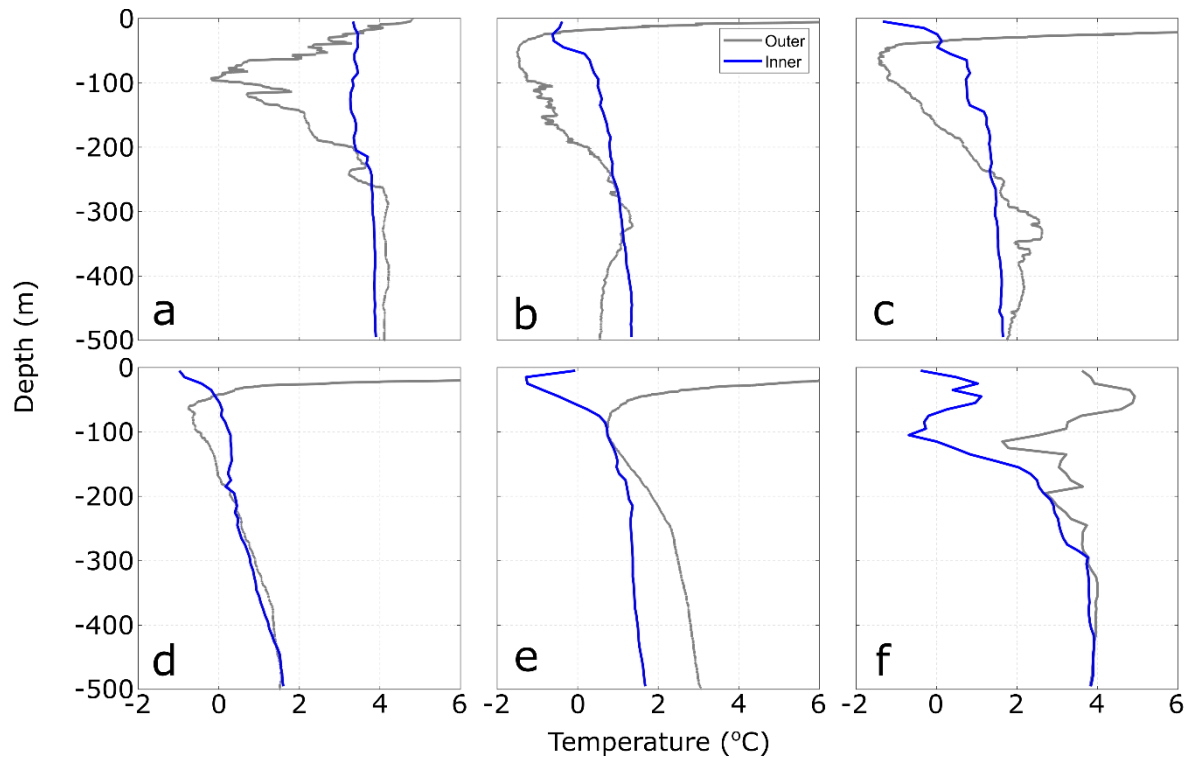


Figure 8. Fjord temperature profiles from the Oceans Melting Greenland project (<https://omg.jpl.nasa.gov/>). The blue lines are profiles acquired within the fjord, close to tidewater glacier termini, and the grey lines are acquired at or beyond the fjord mouth. Fjords (or nearest glacier) shown are (a) Sermilik Fjord, (b) Daugaard-Jensen, (c) Upernavik Isstrom, (d) Nunatakassaap Sermia Fjord, (e) Ilulissat Isfjord, and (f) Timmiarmiut Fjord. Data are available from: <https://omg.jpl.nasa.gov/portal/browse/OMGEV-AXCTD/>

348 gradients are shallow, then icebergs can cause cooling over large depth ranges (e.g. Fig. 7c). As one
 349 example, hydrographic observations in Kangerdlugssuaq Fjord showed relatively uniform near-glacier
 350 temperatures with substantial cooling in both the upper 100 m and between 300 and 400 m depth,
 351 relative to a transect acquired at the fjord mouth (Straneo et al., 2012), consistent with the modelling
 352 results presented here. Iceberg-melt-induced warming of parts of the water column is harder still to
 353 identify in published hydrographic observations because of the difficulty in distinguishing it from
 354 relatively warm subglacial ~~runoff~~discharge-driven plume outflow.

355 To further compare our modelling results to observations, we examined CTD casts acquired as part of
 356 the Oceans Melting Greenland (OMG) project (<https://omg.jpl.nasa.gov/>; data available at:
 357 <https://omg.jpl.nasa.gov/portal/browse/OMGEV-AXCTD/>). ~~As with the previous comparisons, and~~
 358 ~~in~~ keeping with our simulation design, we selected pairs of CTD casts acquired less than a week apart,
 359 one near or outside the fjord mouth and the other as close as possible to the tidewater glacier at the head
 360 of the fjord. These profiles (Fig. 8) show many of the characteristics that we have simulated here.
 361 Specifically, the profiles show that near-surface water temperatures are substantially colder adjacent to
 362 tidewater glaciers compared to those observed outside each fjord, and the observed temperature

363 differences [between the mouth and near-glacier region](#) are comparable to those simulated here. In all
364 but two [of the surveyed fjords](#) (Illulissat Isfjord and Timmiarmiut Fjord) ~~of the surveyed fjords, shown~~
365 [in Figs. 8e & f](#)), the profiles also show warming at intermediate depths (~50-200 m) relative to the
366 waters outside the fjord, [consistent with our simulations using icebergs scenarios three to five,](#)
367 [particularly using our AWwarm boundary conditions \(Figs. 6c-e\)](#). These observations do not allow us
368 to quantify the relative contributions to intermediate depth warming between plume outflow and iceberg
369 melt-induced upwelling. However, we note that the vertical pattern and magnitudes of intermediate
370 depth warming are similar to those simulated here. In addition, the intermediate depth warming occurs
371 over a large depth range, which is not easily explained by plume outflow and is consistent with our
372 simulations. Some of the profiles also show notable cooling at depth (e.g. Illulissat Isfjord, [Fig. 8e](#)),
373 which we are only able to reproduce in simulations including a shallow sill- [\(e.g. the red line in Fig. 4j\)](#).
374 Our simulations may underestimate cooling at depth because power law size-frequency distributions
375 underestimate the number of very large icebergs (Sulak et al., 2017) and because the parameter values
376 used in our melt calculation may underestimate submarine melt rates (Jackson et al., 2020).

377 [In our simulations, we have generally considered a glacier-fjord system in which the glacier face and](#)
378 [subglacial discharge interact with the entire water column, and with icebergs affecting a range of depths](#)
379 [between the surface and their keels, which is a coarse representation of many fjords in Greenland. In](#)
380 [many other fjords in Greenland, glacier grounding lines are shallower, such that the calving front and](#)
381 [subglacial discharge interact predominately with the surface and PW layers. Although our simulations](#)
382 [do not encompass this geometry, they still provide some insights into the potential effect of icebergs on](#)
383 [near-glacier conditions in these fjords. With this geometry, subglacial discharge is injected directly into](#)
384 [the PW layer. Therefore, plume outflow is relatively cool and we would expect, based the simulations](#)
385 [presented here, that iceberg-driven cooling of the surface layer to be significant \(resembling Fig. 3a-c\).](#)
386 [In addition, icebergs calved from such shallow glaciers would not be able to cause upwelling of warm](#)
387 [AW \(as in our scenarios 1 and 2\), and so we would not expect any iceberg melt-driven warming of the](#)
388 [PW layer. Overall, we expect, based on the insights gained from our simulations, that the effect of](#)
389 [iceberg melt on near-glacier water properties in shallow fjords therefore largely manifest as a cooling](#)
390 [in the upper several tens of meters of the water column, thereby reducing vertical variations in water](#)
391 [column temperature. Such patterns have been observed in fjords hosting glaciers with relatively shallow](#)
392 [\(~250 m\) grounding lines resting in the PW layer \(e.g. Mortensen et al., 2020\).](#)

393

394 **4.2. Implications for glacier-ocean interaction**

395 If iceberg-induced changes to glacier-adjacent water properties significantly affect the magnitude
396 and/or the vertical pattern of glacier submarine melting, then icebergs may play an important role in
397 modifying glacier response to ocean forcing. To assess the effect of icebergs on glacier submarine

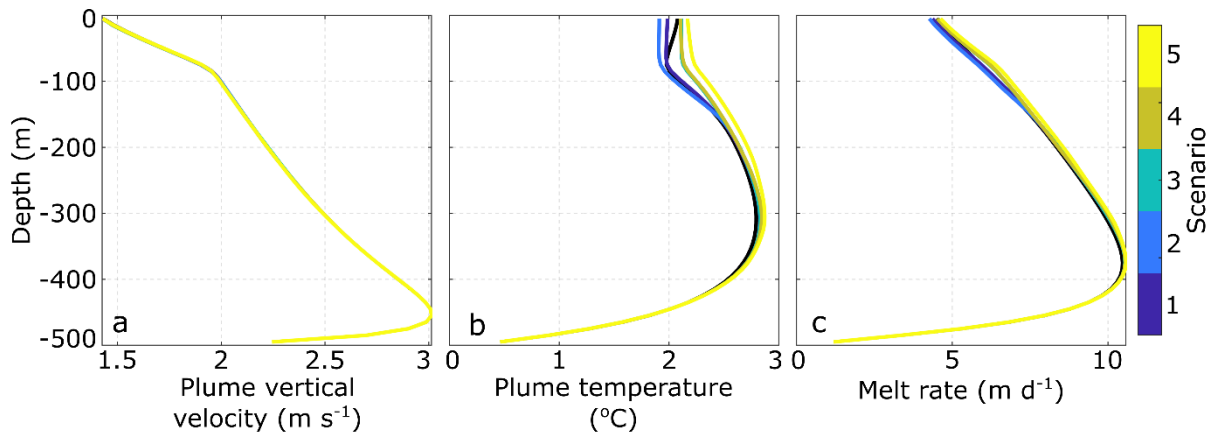


Figure 9. Plume dynamics for iceberg scenarios one to five. (a) Plume vertical velocity. (b) Plume temperature. (c) Glacier submarine melt rate in the plume. All simulations are based on *BCstandard* boundary conditions and 500 m s^{-1} subglacial discharge.

398 melting, we first consider how iceberg-melt impacts subglacial runoff-driven plume dynamics
 399 and then assess how the simulated temperature changes could affect melt rates across the parts of glacier
 400 fronts that are not directly affected by runoff-driven plumes.

401 To examine the effect of icebergs on subglacial discharge plume-driven glacier submarine melting, we
 402 evaluate plume properties for a single set of ocean boundary conditions (*BCstandard*; Fig. 1b-d) using
 403 each of the five iceberg scenarios. We find that submarine iceberg melting has negligible influence on
 404 plume vertical velocity and only modest influence on plume temperature, meaning plume-induced
 405 glacier submarine melt rates appear relatively insensitive to the changes in temperature and salinity
 406 induced by changes in iceberg geometry, concentration and size-frequency distribution (Fig. 9).

407 Although runoff-driven plume dynamics appear to be relatively insensitive to
 408 iceberg-induced modification of glacier-adjacent water properties, submarine melting distal to glacial
 409 plumes ('background melting' (e.g. Slater et al., 2018)) may be more directly affected. Qualitatively,
 410 the iceberg-melt-induced changes to glacier-adjacent water properties presented above suggest that
 411 iceberg melt will affect background glacier melt rates in three key ways: (1) at and near the fjord surface,
 412 cooling will reduce background melt rates; (2) in the PW layer, background melting will usually
 413 increase due to upwelling of warmer AW, and; (3) in the AW layer, iceberg melt-induced changes in
 414 background melt rates are expected to be modest, with slight increases in fjords with steep vertical
 415 temperature gradients, and slight decreases in other fjords (assuming icebergs penetrate into the AW
 416 layer). These effects will be more pronounced in fjords with higher concentrations of larger (and thus
 417 deeper keeled) icebergs. In some fjords, then, where icebergs cause cooling near the surface and
 418 warming at depth, we expect icebergs will increase glacier undercutting through impacting submarine
 419 melt rates, which may in turn influence the rate and mechanism of calving (Benn et al., 2017; James et
 420 al., 2014; O'Leary and Christoffersen, 2013).

421 To explore these effects quantitatively, we calculate the percentage change in background melt rate of
 422 the glacier terminus due to iceberg-induced modification of glacier-adjacent water temperature (relative
 423 to simulations without icebergs). Modelling studies indicate that background melt rates scale linearly
 424 with ocean temperature (Sciascia et al., 2013; Slater et al., 2016; Xu et al., 2013); thus, changes in
 425 temperature, T , should cause proportional changes in background melting (Jackson et al., 2014). We
 426 choose to focus on relative changes in melt rate, rather than absolute changes, because of poor
 427 constraints on important melt rate parameter values (Jackson et al., 2020). We calculate the relative
 428 change in submarine melt rate, SMR , following Jackson et al. (2014), as:

$$429 \quad \Delta SMR = \frac{(T_{ib} - T_f) - (T_{nib} - T_f)}{(T_{nib} - T_f)} 100$$

430 where the subscripts ib and nib indicate simulations with ‘icebergs’ and ‘no icebergs’, respectively, and
 431 T_f is the *in-situ* freezing point, given by:

$$432 \quad T_f = \lambda_1 S + \lambda_2 + \lambda_3 z$$

433 where λ_{1-3} are constants representing the freezing point slope ($-0.0573 \text{ }^\circ\text{C psu}^{-1}$), offset (0.0832°C) and
 434 depth ($0.000761^\circ\text{C m}^{-1}$), respectively. (Cowton et al., 2015). S is the local salinity (horizontally
 435 averaged within 2 km of the terminus) and z is depth in the water column. It is worth noting that changes
 436 in melt rate calculated using this method assume that all changes in heat supply are accommodated by
 437 changes in submarine melt rates, and so this method provides an indication of the maximum relative
 438 changes in submarine melt rates expected due to changes in ambient ocean temperature.

439 Using this approach, we find that the impact on water properties resulting from iceberg melt
 440 substantially modifies background glacier submarine melt rates. Firstly, in the upper 50 m and using
 441 *BCstandard*, iceberg melt causes a 34.9% reduction in melt rate on average. Even in iceberg scenario
 442 one, iceberg melt causes a 29.5% reduction in melt rate over this depth range. Secondly, between 100
 443 and 200 m depth, iceberg melt causes a 13.5% increase in melt rate on average when using *BCstandard*,
 444 but this increases to 59.2% when using *PWcool* (for which warming of the PW layer due to upwelling
 445 is most pronounced). Changes in iceberg melt rates in the AW layer are minimal, with the most
 446 pronounced effect being a 5.4% increase in the 200-400 m depth range using iceberg scenario five and
 447 *PWwarm*. When averaged through the entire water column, these effects largely compensate for each
 448 other, resulting in a net 3.1% decrease in melt rates with *BCstandard*. Overall therefore, this analysis
 449 suggests that iceberg melt can influence the vertical pattern of glacier terminus background melting by
 450 decreasing melt rates at the surface and increasing them in the PW layer, with minimal changes in the
 451 AW layer.

452 As well as affecting glacier-adjacent water temperatures, iceberg melt likely affects submarine melt
 453 rates in other ways not examined here. For example, the cooling and freshening of the surface and near-

454 surface layers induced by iceberg melting may prevent or hinder plume surfacing (De Andrés et al.,
455 2020), and may expedite sea ice formation after the melt season, promoting the development of an ice
456 mélange. In addition, mechanical iceberg breakup, iceberg calving and iceberg rotation can cause
457 vigorous mixing of fjord waters which can temporarily increase glacier and iceberg submarine melt
458 rates (Enderlin et al., 2018), and increases the iceberg-ocean contact area available for melting. Iceberg-
459 melt-induced invigoration of fjord circulation can increase oceanic heat flux towards tidewater glaciers
460 (Davison et al., 2020), likely resulting in faster terminus submarine melting. Icebergs likely also exert
461 a mechanical influence on the circulation and plume dynamics at the ice-ocean interface (Amundson et
462 al., 2020), and may prevent plume surfacing (Xie et al., 2019).

463

464 **4.3. Implications for oceanic forcing of ice sheet-scale models**

465 Current state-of-the-art projections of dynamic mass loss from the Greenland Ice Sheet (Goelzer et al.,
466 2020) are forced by far-field ocean temperature profiles, provided by ocean modelling output that does
467 not include fjord-scale processes (except for the obstruction of shelf-water intrusion by shallow sills)
468 (Slater et al., 2019, 2020). The results presented here suggest that such an approach is broadly
469 appropriate for fjords with maximum iceberg keel depths of less than 200 m and iceberg concentrations
470 less than ~20% on average, where iceberg modification of glacier-adjacent water properties appears to
471 be limited other than in the upper several tens of metres (Figs 4 and 6). The majority of Greenland's
472 fjords likely fall into this category (Mankoff et al., 2019; Sulak et al., 2017). Even in such fjords,
473 however, this approach would not capture the surface and near-surface cooling caused by iceberg
474 melting. In order to capture this near surface cooling, one relatively simple modification to such an
475 approach could be to reduce surface water temperature to close to the *in-situ* melting point during winter
476 periods, and proportionally to the iceberg surface area at the fjord surface during summer periods.

477 However, in fjords hosting icebergs with keel depth greater than or equal to 200 m and with average
478 concentrations of more than ~20% (i.e. our iceberg scenario three or higher), iceberg modification of
479 glacier-adjacent water properties becomes increasingly important. In such fjords that also exhibit
480 relatively shallow sills, icebergs act to cool glacier-adjacent water throughout the water column, with
481 the amount of cooling proportional to the draught and concentration of the icebergs, as well as to the
482 temperature of the ambient water at the fjord mouth (Fig. 4). In such fjords that do not have shallow
483 sills, the effect is more complicated, with both iceberg-melt-induced warming and cooling, depending
484 on the vertical temperature gradient of the water column and iceberg concentration at depth. Overall,
485 these changes to the water column temperature can cause non-negligible (up to several tens of percent)
486 changes in terminus submarine melt rates across the large areas of the calving front that are not directly
487 affected by plume-inducing subglacial discharge. The vertical pattern of changes to terminus submarine
488 melt rates (reduced near the surface and increased at intermediate depths) induced by iceberg melting

489 is expected to exacerbate undercutting of glacier termini, with potentially important impacts on calving
490 rates (Benn et al., 2017; Ma and Bassis, 2019; O’Leary and Christoffersen, 2013; Todd and
491 Christoffersen, 2014). Although fjords hosting icebergs this large and numerous are relatively few in
492 number, it is these fjords (and the glaciers hosted by them) that contribute the most to dynamic mass
493 loss from the Greenland Ice Sheet (Enderlin et al., 2014; Khan et al., 2020).

494

495 **4.4. Transience vs steady-state**

496 All of the results presented here were extracted from the final ten days of simulations that were run to
497 a quasi-steady state (i.e. the variable of interest had stabilised). In our domains without sills, steady-
498 state of temperature and salinity was generally reached after just ten to thirty days. However, our
499 simulations with sills could take as many as one thousand days to reach such a steady state because
500 fjord-shelf exchange is reduced. For an equivalent steady-state to be reached in reality, open ocean
501 conditions, [runoffsubglacial discharge](#) and iceberg size and distribution would also have to remain
502 quasi-stable for an equivalent time period. In reality, this is unlikely to occur (particularly in fjords with
503 shallow sills) because [runoffsubglacial discharge](#) and coastal and open ocean conditions change on sub-
504 seasonal to seasonal timescales (Moon et al., 2017; Mortensen et al., 2014; Noël et al., 2016; Sutherland
505 et al., 2014; Sutherland and Pickart, 2008). In reality therefore, glacier-adjacent water properties in
506 fjords with shallow sills are likely a complex amalgamation of temporally-evolving source waters,
507 modified by processes operating within the fjord. In addition, some variations in coastal conditions can
508 be transmitted towards glaciers very rapidly. During winter, strong wind events on the east coast of
509 Greenland drive fast shelf-forced flows (or intermediary currents) in glacial fjords, delivering coastal
510 waters to tidewater glaciers over just a period of a few days, and potentially reducing the magnitude of
511 iceberg-driven modification (Jackson et al., 2014, 2018). Such currents are strongest in winter, when
512 hydrographic observations are sparse, so this remains speculative.

513

514 **5. Conclusions**

515 We have used a general circulation model (MITgcm) to quantify the effect of submarine iceberg melting
516 on glacier-adjacent water properties in an idealised fjord domain. A large range of iceberg
517 concentrations, keel depths and size-frequency distributions were examined to represent the range of
518 iceberg conditions found in Greenland’s marine terminating glacier fjords. We focused primarily on
519 iceberg_melt-induced changes to glacier-adjacent water temperatures throughout the water column,
520 because of their principal importance to glacier-submarine melting.

521 Our results suggest that icebergs can substantially modify glacier-adjacent water properties and that the
522 precise impact depends on iceberg size and on the temperature profile and stratification of water within
523 and beyond the fjord. In particular, we find that (1) temperature in the upper ~60 m of the water column

524 is reduced by several degrees Celsius over a wide range of iceberg scenarios; (2) fjords with more and
525 deeper icebergs are subject to greater iceberg_melt-induced modification, which can result in either
526 cooling or warming at different depths depending on the balance between melt-driven cooling and
527 upwelling-driven warming, which in turn depends on fjord temperature stratification, and; (3) when
528 icebergs extend to or below the fjord mouth sill depth, they can cause significant cooling throughout
529 the water column. Particularly with regard to point (2), our results highlight that oceanic forcing of large
530 fast-flowing glaciers, which contribute the most to ice sheet dynamic mass loss, in existing projections
531 of tidewater glacier dynamics is strongly affected by ignoring the impact of icebergs on fjord water
532 properties. The iceberg-induced changes to the vertical temperature profile of glacier-adjacent waters
533 identified here are likely to reduce submarine melt rates at and near the fjord surface while increasing
534 them in the PW layer, which may influence the rate and mechanism of calving by exacerbating glacier
535 terminus undercutting. Our results therefore identify a critical need to develop simple parameterisations
536 of iceberg-induced modification of fjord waters, and other fjord-scale processes, to better constrain
537 oceanic forcing of tidewater glaciers.

538

539

540 **Code availability**

541 MITgcm is freely available at http://mitgcm.org/public/source_code.html. The IcePlume module is
542 available from Tom Cowton on request. The IceBerg module is available at
543 <https://zenodo.org/record/3979647#.YWAayNrMKUk> or from Benjamin Davison on request.

544

545 **Data availability**

546 Data required to reproduce the analysis and figures in this manuscript will be made available upon
547 publication.

548

549 **Author contributions**

550 BD and TC conceived the study. BD developed the model code with support from TC and AS. BD
551 designed and conducted the simulations and analysis, and led the manuscript write up. TC, FC, AS and
552 PN supported the interpretation of the model results and contributed to the preparation of the
553 manuscript.

554

555 **Competing interests**

556 The authors declare that they have no conflict of interest.

557

558 **Acknowledgements**

559 BD was funded by a PhD studentship provided by the Scottish Alliance for Geosciences, Environment
560 and Society (SAGES) and the University of St Andrews, UK. The simulations were conducted on the
561 Sheffield Advanced Research Computer (ShARC).

562 **References**

563 Amundson, J. M., Kienholz, C., Hager, A. O., Jackson, R. H., Motyka, R. J., Nash, J. D. and
564 Sutherland, D. A.: Formation, flow and break-up of ephemeral ice mélange at LeConte Glacier and
565 Bay, Alaska, *J. Glaciol.*, 66(258), 577–590, doi:10.1017/jog.2020.29, 2020.

566 De Andrés, E., Slater, D. A., Straneo, F., Otero, J., Das, S. and Navarro, F.: Surface emergence of
567 glacial plumes determined by fjord stratification, *Cryosph. Discuss.*, in review(January),
568 doi:<https://doi.org/10.5194/tc-2019-264>, 2020.

569 Barker, A., Sayed, M. and Carrieres, T.: Determination of iceberg draft, mass and cross-sectional
570 areas, *Proc. 14th Int. Offshore Polar Eng. Conf.*, 899–904, 2004.

571 Beard, N., Straneo, F. and Jenkins, W.: Characteristics of meltwater export from Jakobshavn Isbræ
572 and Ilulissat Icefjord, *Ann. Glaciol.*, 58(74), 107–117, doi:10.1017/aog.2017.19, 2017.

573 Beard, N. L., Straneo, F. and Jenkins, W.: Export of Strongly Diluted Greenland Meltwater From a
574 Major Glacial Fjord, *Geophys. Res. Lett.*, 45(9), 4163–4170, doi:10.1029/2018GL077000, 2018.

575 Benn, D. I., Aström, J., Zwinger, T., Todd, J., Nick, F. M., Cook, S., Hulton, N. R. J. and Luckman,
576 A.: Melt-under-cutting and buoyancy-driven calving from tidewater glaciers: New insights from
577 discrete element and continuum model simulations, *J. Glaciol.*, 63(240), 691–702,
578 doi:10.1017/jog.2017.41, 2017.

579 Carroll, D., Sutherland, D. A., Hudson, B., Moon, T., Catania, G. A., Shroyer, E. L., Nash, J. D.,
580 Bartholomäus, T. C., Felikson, D., Stearns, L. A., Noël, Y. and Van Den Broeke, M. R.: The impact
581 of glacier geometry on meltwater plume structure and submarine melt in Greenland fjords, *Geophys.*
582 *Res. Lett.*, 43, doi:10.1002/2016GL070170, 2016.

583 Cowton, T., Slater, D., Sole, A., D, G. and Nienow, P.: Modeling the impact of glacial runoff on
584 fjord circulation and submarine melt rate using a new subgrid-scale parameterization for glacial
585 plumes, *J. Geophys. Res. Ocean.*, 120, 1–17, doi:10.1002/2014JC010324, 2015.

586 Cowton, T., Sole, A., Nienow, P., Slater, D., Wilton, D. and Hanna, E.: Controls on the transport of

587 oceanic heat to Kangerdlugssuaq Glacier, East Greenland, *J. Glaciol.*, 1–14,
588 doi:10.1017/jog.2016.117, 2016.

589 Davison, B. J., Cowton, T. R., Cottier, F. R. and Sole, A. J.: Iceberg melting substantially modifies
590 oceanic heat flux towards a major Greenlandic tidewater glacier, *Nat. Commun.*, 11(1), 1–13,
591 doi:10.1038/s41467-020-19805-7, 2020.

592 Dowdeswell, J. A., Whittington, R. J. and Hodgkins, R.: The sizes, frequencies, and freeboards of
593 East Greenland icebergs observed using ship radar and sextant, *J. Geophys. Res.*, 97(C3), 3515,
594 doi:10.1029/91JC02821, 1992.

595 Edwards, T. L., Nowicki, S., Marzeion, B., Hock, R., Goelzer, H., Seroussi, H., Jourdain, N. C.,
596 Slater, D. A., Turner, F. E., Smith, C. J., McKenna, C. M., Simon, E., Abe-Ouchi, A., Gregory, J. M.,
597 Larour, E., Lipscomb, W. H., Payne, A. J., Shepherd, A., Agosta, C., Alexander, P., Albrecht, T.,
598 Anderson, B., Asay-Davis, X., Aschwanden, A., Barthel, A., Bliss, A., Calov, R., Chambers, C.,
599 Champollion, N., Choi, Y., Cullather, R., Cuzzone, J., Dumas, C., Felikson, D., Fettweis, X., Fujita,
600 K., Galton-Fenzi, B. K., Gladstone, R., Golledge, N. R., Greve, R., Hattermann, T., Hoffman, M. J.,
601 Humbert, A., Huss, M., Huybrechts, P., Immerzeel, W., Kleiner, T., Kraaijenbrink, P., Le clec'h, S.,
602 Lee, V., Leguy, G. R., Little, C. M., Lowry, D. P., Malles, J. H., Martin, D. F., Maussion, F.,
603 Morlighem, M., O'Neill, J. F., Nias, I., Pattyn, F., Pelle, T., Price, S. F., Quiquet, A., Radić, V.,
604 Reese, R., Rounce, D. R., Rückamp, M., Sakai, A., Shafer, C., Schlegel, N. J., Shannon, S., Smith, R.
605 S., Straneo, F., Sun, S., Tarasov, L., Trusel, L. D., Van Breedam, J., van de Wal, R., van den Broeke,
606 M., Winkelmann, R., Zekollari, H., Zhao, C., Zhang, T. and Zwinger, T.: Projected land ice
607 contributions to twenty-first-century sea level rise, *Nature*, 593(7857), 74–82, doi:10.1038/s41586-
608 021-03302-y, 2021.

609 Enderlin, E. M., Howat, I. M., Jeong, S., Noh, M. J., van Angelen, J. H. and Van den Broeke, M. R.:
610 An improved mass budget for the Greenland ice sheet, *Geophys. Res. Lett.*, 41, 866–872,
611 doi:10.1002/2013GL059010., 2014.

612 Enderlin, E. M., Hamilton, G. S., Straneo, F. and Sutherland, D. A.: Iceberg meltwater fluxes
613 dominate the freshwater budget in Greenland's iceberg-congested glacial fjords, *Geophys. Res. Lett.*,
614 43(21), 11,287-11,294, doi:10.1002/2016GL070718, 2016.

615 Enderlin, E. M., Carrigan, C. J., Kochtitzky, W. H., Cuadros, A., Moon, T. and Hamilton, G. S.:
616 Greenland Iceberg Melt Variability from High-Resolution Satellite Observations, *Cryosph.*,
617 (September), 1–17, 2018.

618 Fenty, I., Willis, J., Khazendar, A., Dinardo, S., Forsberg, R., Fukumori, I., Holland, D., Jakobsson,
619 M., Moller, D., Morison, J., Münchow, A., Rignot, E., Schodlok, M., Thompson, A., Tinto, K.,
620 Rutherford, M. and Trenholm, N.: Oceans Melting Greenland: Early Results from NASA's Ocean-Ice

621 Mission in Greenland, *Oceanography*, 29(4), 72–83, doi:10.5670/oceanog.2016.100, 2016.

622 Fraser, N. J. and Inall, M. E.: Influence of Barrier Wind Forcing on Heat Delivery Toward the
623 Greenland Ice Sheet, *J. Geophys. Res. Ocean.*, 123(4), 2513–2538, doi:10.1002/2017JC013464, 2018.

624 Gladish, C. V., Holland, D. M., Rosing-Asvid, A., Behrens, J. W. and Boje, J.: Oceanic Boundary
625 Conditions for Jakobshavn Glacier: Part I. Variability and Renewal of Ilulissat Icefjord Waters, 2001-
626 2014, *J. Phys. Oceanogr.*, 45, doi:10.1175/JPO-D-14-0044.1, 2015.

627 Goelzer, H., Nowicki, S., Payne, A., Larour, E., Seroussi, H., Lipscomb, W. H., Gregory, J., Abe-
628 Ouchi, A., Shepherd, A., Simon, E., Agosta, C., Alexander, P., Aschwanden, A., Barthel, A., Calov,
629 R., Chambers, C., Choi, Y., Cuzzone, J., Dumas, C., Edwards, T., Felikson, D., Fettweis, X.,
630 Golledge, N. R., Greve, R., Humbert, A., Huybrechts, P., Le Clec'H, S., Lee, V., Leguy, G., Little, C.,
631 Lowry, D., Morlighem, M., Nias, I., Quiquet, A., Rückamp, M., Schlegel, N. J., Slater, D. A., Smith,
632 R., Straneo, F., Tarasov, L., Van De Wal, R. and Van Den Broeke, M.: The future sea-level
633 contribution of the Greenland ice sheet: A multi-model ensemble study of ISMIP6, *Cryosphere*, 14(9),
634 3071–3096, doi:10.5194/tc-14-3071-2020, 2020.

635 [Hellmer, H., and Olbers, D.: A two-dimensional model for the thermohalin circulation under an ice](#)
636 [shelf, *Antarct. Sci.*, 325-336, doi: 10.1017/S0954102089000490, 1989.](#)

637 Holland, D. M. and Jenkins, A.: Modeling Thermodynamic Ice–Ocean Interactions at the Base of an
638 Ice Shelf, *J. Phys. Oceanogr.*, 29(8), 1787–1800, doi:10.1175/1520-
639 0485(1999)029<1787:MTIOIA>2.0.CO;2, 1999.

640 Inall, M. E., Murray, T., Cottier, F. R., Scharrer, K. and Boyd, T. J.: Oceanic heat delivery via
641 Kangerdlugssuaq Fjord to the south-east Greenland ice sheet, *J. Geophys. Res. Ocean.*, 631–645,
642 doi:10.1002/2013JC009295. [Received](#), 2014.

643 Jackson, R. H. and Straneo, F.: Heat, salt, and freshwater budgets for a glacial fjord in Greenland, *J.*
644 *Phys. Oceanogr.*, 0(0), 2735–2768, doi:10.1175/JPO-D-15-0134.1, 2016.

645 Jackson, R. H., Straneo, F. and Sutherland, D. a.: Externally forced fluctuations in ocean temperature
646 at Greenland glaciers in non-summer months, *Nat. Geosci.*, 7(June), 1–6, doi:10.1038/ngeo2186,
647 2014.

648 Jackson, R. H., Shroyer, E. L., Nash, J. D., Sutherland, D. A., Carroll, D., Fried, M. J., Catania, G. A.,
649 Bartholomaus, T. C. and Stearns, L. A.: Near-glacier surveying of a subglacial discharge plume:
650 Implications for plume parameterizations, *Geophys. Res. Lett.*, 44(13), 6886–6894,
651 doi:10.1002/2017GL073602, 2017.

652 Jackson, R. H., Lentz, S. J. and Straneo, F.: The dynamics of shelf forcing in Greenlandic fjords, *J.*

653 Phys. Oceanogr., 48(11), 2799–2827, doi:10.1175/JPO-D-18-0057.1, 2018.

654 Jackson, R. H., Nash, J. D., Kienholz, C., Sutherland, D. A., Amundson, J. M., Motyka, R. J.,
655 Winters, D., Skyllingstad, E. and Pettit, E. C.: Meltwater Intrusions Reveal Mechanisms for Rapid
656 Submarine Melt at a Tidewater Glacier, *Geophys. Res. Lett.*, 47(2), doi:10.1029/2019GL085335,
657 2020.

658 Jakobsson, M., Mayer, L. A., Nilsson, J., Stranne, C., Calder, B., O’Regan, M., Farrell, J. W., Cronin,
659 T. M., Brüchert, V., Chawarski, J., Eriksson, B., Fredriksson, J., Gemery, L., Glueder, A., Holmes, F.
660 A., Jerram, K., Kirchner, N., Mix, A., Muchowski, J., Prakash, A., Reilly, B., Thornton, B., Ulfso,
661 A., Weidner, E., Åkesson, H., Handl, T., Ståhl, E., Boze, L.-G., Reed, S., West, G. and Padman, J.:
662 Ryder Glacier in northwest Greenland is shielded from warm Atlantic water by a bathymetric sill,
663 *Commun. Earth Environ.*, 1(1), 1–10, doi:10.1038/s43247-020-00043-0, 2020.

664 James, T. D., Murray, T., Selmes, N., Scharrer, K. and O’Leary, M.: Buoyant flexure and basal
665 crevassing in dynamic mass loss at Helheim Glacier, *Nat. Geosci.*, 7(8), 593–596,
666 doi:10.1038/ngeo2204, 2014.

667 Jenkins, A.: Convection-Driven Melting near the Grounding Lines of Ice Shelves and Tidewater
668 Glaciers, *J. Phys. Oceanogr.*, 41(12), 2279–2294, doi:10.1175/JPO-D-11-03.1, 2011.

669 Khan, S. A., Bjørk, A. A., Bamber, J. L., Morlighem, M., Bevis, M., Kjær, K. H., Mougnot, J.,
670 Løkkegaard, A., Holland, D. M., Aschwanden, A., Zhang, B., Helm, V., Korsgaard, N. J., Colgan, W.,
671 Larsen, N. K., Liu, L., Hansen, K., Barletta, V., Dahl-Jensen, T. S., Søndergaard, A. S., Csatho, B.
672 M., Sasgen, I., Box, J. and Schenk, T.: Centennial response of Greenland’s three largest outlet
673 glaciers, *Nat. Commun.*, 11(1), 1–9, doi:10.1038/s41467-020-19580-5, 2020.

674 Kimura, S., Holland, P. R., Jenkins, A. and Piggott, M.: The effect of meltwater plumes on the
675 melting of a vertical glacier face, *J. Phys. Oceanogr.*, 44(12), 3099–3117, doi:10.1175/JPO-D-13-
676 0219.1, 2014.

677 Luthi, M., Funk, M., Iken, A., Gogineni, S. and Truffer, M.: Mechanisms of fast flow in Jakobshavn
678 Isbræ, Greenland, Part III: Measurements of ice deformation, temperature and cross-
679 borehole conductivity in boreholes to the bedrock, *J. Glaciol.*, 48(162), 369–385,
680 doi:10.3189/172756502781831322, 2002.

681 Ma, Y. and Bassis, J. N.: The Effect of Submarine Melting on Calving From Marine Terminating
682 Glaciers, *J. Geophys. Res. Earth Surf.*, 124(2), 334–346, doi:10.1029/2018JF004820, 2019.

683 Mankoff, K. D., Solgaard, A., Colgan, W., Ahlstrøm, A. P., Abbas Khan, S. and Fausto, R. S.:
684 Greenland Ice Sheet solid ice discharge from 1986 through March 2020, *Earth Syst. Sci. Data*, 12(2),
685 1367–1383, doi:10.5194/essd-12-1367-2020, 2019.

686 Mankoff, K. D., Noël, B., Fettweis, X., Ahlstrøm, A. P., Colgan, W., Kondo, K., Langley, K.,
687 Sugiyama, S., Van As, D. and Fausto, R. S.: Greenland liquid water discharge from 1958 through
688 2019, *Earth Syst. Sci. Data*, 12(4), 2811–2841, doi:10.5194/essd-12-2811-2020, 2020.

689 Marshall, J., Adcroft, A., Hill, C., Perelman, L. and Heisey, C.: A finite-volume, incompressible
690 Navier Stokes model for studies of the ocean on parallel computers, *J. Geophys. Res.*, 102(C3), 5753,
691 doi:10.1029/96JC02775, 1997a.

692 Marshall, J., Hill, C., Perelman, L. and Adcroft, A.: Hydrostatic, quasi-hydrostatic, and
693 nonhydrostatic ocean modeling, *J. Geophys. Res.*, 102(C3), 5733, doi:10.1029/96JC02776, 1997b.

694 Meredith, M., Sommerkorn, M., Cassotta, S., Derksen, C., Ekaykin, A., Hollowed, A., Kofinas, G.,
695 Mackintosh, A., Melbourne-Thomas, J., Muelbert, M. M. C., Ottersen, G., Pritchard, H. and Schuur,
696 E. A. G.: Special Report on Ocean and Cryosphere in a Changing Climate: Polar Regions, , 203–320,
697 doi:10.1016/S1366-7017(01)00066-6, 2020.

698 Moon, T., Sutherland, D. A., Carroll, D., Felikson, D., Kehrl, L. and Straneo, F.: Subsurface iceberg
699 melt key to Greenland fjord freshwater budget, *Nat. Geosci.*, doi:10.1038/s41561-017-0018-z, 2017.

700 Mortensen, J., Bendtsen, J., Lennert, K. and Rysgaard, S.: Seasonal variability of the circulation
701 system in a west Greenland tidewater outlet glacier fjord, Godthåbsfjord (64°N), *J. Geophys. Res.*
702 *Earth Surf.*, 2591–2603, doi:10.1002/2014JF003267., 2014.

703 [Mortensen, J., Rysgaard, S., Bendtsen, J., Lennert, K., Kanzow, T., Lund, H., and Meire, L.:](#)
704 [Subglacial discharge and its down-fjord transformation in West Greenland with an ice melange. *JGR:*](#)
705 [Oceans, 125, e2020JC016301. doi:10.1029/2020JC016301, 2020.](#)

706 Moyer, A. N., Sutherland, D. A., Nienow, P. W. and Sole, A. J.: Seasonal Variations in Iceberg
707 Freshwater Flux in Sermilik Fjord, Southeast Greenland From Sentinel-2 Imagery, *Geophys. Res.*
708 *Let.*, 46(15), 8903–8912, doi:10.1029/2019GL082309, 2019.

709 Noël, B., Berg, W. J. Van De, Machguth, H., Lhermitte, S., Howat, I. and Fettweis, X.: A daily , 1 km
710 resolution dataset of downscaled Greenland ice sheet surface mass balance (1958-2015), *Cryosph.*
711 *Discuss.*, (May), 1–29, doi:10.5194/tc-2016-145, 2016.

712 O’Leary, M. and Christoffersen, P.: Calving on tidewater glaciers amplified by submarine frontal
713 melting, *Cryosphere*, 7, 119–128, doi:10.5194/tc-7-119-2013, 2013.

714 Rezvanbehbahani, S., Stearns, L. A., Keramati, R., Shankar, S. and van der Veen, C. J.: Significant
715 contribution of small icebergs to the freshwater budget in Greenland fjords, *Commun. Earth Environ.*,
716 1(1), 1–7, doi:10.1038/s43247-020-00032-3, 2020.

717 [Schaffer, J., Kanzow, T., von Appen, W.-J., von Albedyll, L., Arndt, J. E., and Roberts, D. H.:](#)

718 [Bathymetry constrains ocean heat supply to Greenland's largest glacier tongue, Nat. Geosci., doi:](#)
719 [10.1038/s41561-019-0529-x. 2020.](#)

720 Sciascia, R., Straneo, F., Cenedese, C. and Heimbach, P.: Seasonal variability of submarine melt rate
721 and circulation in an East Greenland fjord, *J. Geophys. Res. Ocean.*, 118(5), 2492–2506,
722 doi:10.1002/jgrc.20142, 2013.

723 Slater, D. A., Nienow, P. W., Cowton, T. R., Goldberg, D. N. and Sole, A. J.: Effect of near-terminus
724 subglacial hydrology on tidewater glacier submarine melt rates, *Geophys. Res. Lett.*, 1–8,
725 doi:10.1002/2014GL062494.1., 2015.

726 Slater, D. A., Goldberg, D. N., Nienow, P. W. and Cowton, T. R.: Scalings for Submarine Melting at
727 Tidewater Glaciers from Buoyant Plume Theory, *J. Phys. Oceanogr.*, 46, 1839–1855,
728 doi:10.1175/JPO-D-15-0132.1, 2016.

729 Slater, D. A., Straneo, F., Das, S. B., Richards, C. G., Wagner, T. J. W. and Nienow, P. W.: Localized
730 Plumes Drive Front-Wide Ocean Melting of A Greenlandic Tidewater Glacier, *Geophys. Res. Lett.*,
731 45(22), 12,350–12,358, doi:10.1029/2018GL080763, 2018.

732 Slater, D. A., Straneo, F., Felikson, D., Little, C. M., Goelzer, H., Fettweis, X. and Holte, J.:
733 Estimating Greenland tidewater glacier retreat driven by submarine melting, *Cryosphere*, 13(9),
734 2489–2509, doi:10.5194/tc-13-2489-2019, 2019.

735 Slater, D. A., Felikson, D., Straneo, F., Goelzer, H., Little, C. M., Morlighem, M., Fettweis, X. and
736 Nowicki, S.: Twenty-first century ocean forcing of the Greenland ice sheet for modelling of sea level
737 contribution, *Cryosphere*, 14(3), 985–1008, doi:10.5194/tc-14-985-2020, 2020.

738 Straneo, F. and Heimbach, P.: North Atlantic warming and the retreat of Greenland's outlet glaciers,
739 *Nature*, 504, 36–43, doi:10.1038/nature12854, 2013.

740 Straneo, F., Hamilton, G. S., Sutherland, D. A., Stearns, L. A., Davidson, F., Hammill, M. O.,
741 Stenson, G. B. and Rosing-Asvid, A.: Rapid circulation of warm subtropical waters in a major glacial
742 fjord in East Greenland, *Nat. Geosci.*, 3(3), 182–186, doi:10.1038/ngeo764, 2010.

743 Straneo, F., Curry, R. G., Sutherland, D. a., Hamilton, G. S., Cenedese, C., Våge, K. and Stearns, L.
744 a.: Impact of fjord dynamics and glacial runoff on the circulation near Helheim Glacier, *Nat. Geosci.*,
745 4(5), 322–327, doi:10.1038/ngeo1109, 2011.

746 Straneo, F., Sutherland, D. a., Holland, D., Gladish, C., Hamilton, G. S., Johnson, H. L., Rignot, E.,
747 Xu, Y. and Koppes, M.: Characteristics of ocean waters reaching Greenland's glaciers, *Ann. Glaciol.*,
748 53(60), 202–210, doi:10.3189/2012AoG60A059, 2012.

749 Sulak, D. J., Sutherland, D. A., Enderlin, E. M., Stearns, L. A. and Hamilton, G. S.: Iceberg properties

750 and distributions in three Greenlandic fjords using satellite imagery, *Ann. Glaciol.*, (May), 1–15,
751 doi:10.1017/aog.2017.5, 2017.

752 Sutherland, D., Straneo, F. and Pickart, R. S.: Characteristics and dynamics of two major greenland
753 glacial fjords, *J. Geophys. Res. Earth Surf.*, 2121–2128, doi:10.1002/jgrc.20224, 2014.

754 Sutherland, D. A. and Pickart, R. S.: The East Greenland Coastal Current: Structure, variability, and
755 forcing, *Prog. Oceanogr.*, 78(1), 58–77, doi:10.1016/j.pocean.2007.09.006, 2008.

756 Sutherland, D. A. and Straneo, F.: Estimating ocean heat transports and submarine melt rates in
757 sermilik fjord, greenland, using lowered acoustic doppler current profiler (LADCP) velocity profiles,
758 *Ann. Glaciol.*, 53(60), 50–58, doi:10.3189/2012AoG60A050, 2012.

759 Sutherland, D. A., Jackson, R. H., Kienholz, C., Amundson, J. M., Dryer, W. P., Duncan, D., Eidam,
760 E. F., Motyka, R. J. and Nash, J. D.: Direct observations of submarine melt and subsurface geometry
761 at a tidewater glacier, *Science* (80-.), 365(6451), 369–374, doi:10.1126/science.aax3528, 2019.

762 Todd, J. and Christoffersen, P.: Are seasonal calving dynamics forced by buttressing from ice
763 mélange or undercutting by melting? Outcomes from full-Stokes simulations of Store Glacier, West
764 Greenland, *Cryosph.*, 8(6), 2353–2365, doi:10.5194/tc-8-2353-2014, 2014.

765 Xie, S., Dixon, T. H., Holland, D. M., Voytenko, D. and Vaňková, I.: Rapid iceberg calving following
766 removal of tightly packed pro-glacial mélange, *Nat. Commun.*, 10(1), doi:10.1038/s41467-019-
767 10908-4, 2019.

768 Xu, Y., Rignot, E., Menemenlis, D. and Koppes, M.: Numerical experiments on subaqueous melting
769 of Greenland tidewater glaciers in response to ocean warming and enhanced subglacial discharge,
770 *Ann. Glaciol.*, 53(60), 229–234, doi:10.3189/2012AoG60A139, 2012.

771 Xu, Y., Rignot, E., Fenty, I., Menemenlis, D. and Flexas, M. M.: Subaqueous melting of Store
772 Glacier, west Greenland from three-dimensional, high-resolution numerical modeling and ocean
773 observations, *Geophys. Res. Lett.*, 40, 4648–4653, doi:10.1002/grl.50825, 2013.

774

775